Civil Engineering Infrastructures Journal, 53(2): 341 – 358, December 2020
Print ISSN: 2322-2093; Online ISSN: 2423-6691
DOI: 10.22059/ceij.2020.285244.1598

Research Paper

Determination of Creep-Induced Displacement of Soil Slopes Based on LEM

Mirzazadeh, Z.[1] and Hajiazizi, M.[2*]

[1] M.Sc. Student, Department of Geotechnical Engineering, Razi University, Kermanshah, Iran.
[2] Associate Professor, Department of Geotechnical Engineering, Razi University, Kermanshah, Iran.

Received: 12 Jul. 2019; Revised: 22 Aug. 2020; Accepted: 25 Aug. 2020

ABSTRACT: The creep of earth slopes is an important challenge of the long-term stability of slopes. This paper develops a limit equilibrium method (LEM)-based analytical approach for calculating the shear displacement of creep-induced failure surface in 2D state for all slices where both force and moment equilibrium equations are simultaneously satisfied as a new research. The relation between shear displacement and creep time is obtained with regard to visco-elastoplastic creep model. The overall safety factor is first calculated for the slip surface using Spencer method. Then, the shear displacements of all slices are obtained based on vertical displacement of crown and using displacement compatibility relation exists between slices. By combining force and moment equilibrium equations and assuming a zero resultant for inter-slice forces, the vertical displacement at crown is determined using visco-elastopastic creep model. A numerical model was developed to calculate slope displacement by the proposed method. Force and moment equilibrium equations are simultaneously satisfied by iteration technique. The proposed method is verified through two numerical examples comparing the new approach and conventional finite element method.

Keywords: Creep, Displacement, Limit Equilibrium, Soil Slope.

INTRODUCTION

Time-dependent behavior of soils has widely been studied using one and three dimensional tests. When a soil subjects to a constant load, it is deformed over time. This deformation is called creep (Augustesen et al., 2004). Cohesive soil slopes show gravity-induced creep due to their viscose behavior (Khaled and Mahmoud, 2018). The creep of the slopes of mountainous regions can lead to landslide and, in turn, financial damages and mortalities (Mohamed et al., 2009; Puzrin and Schmid, 2012). Therefore, predicting creep behavior in slopes is of high importance.

Numerical models can serve as a beneficial tool by adopting a suitable constitutive law for describing the behavior of materials. Primary studies on the long term slopes stability have mainly been founded on the progressive failures of over consolidated clay. Different models have been introduced to model soil creep. The majority of studies are based on simple constitutive models

* Corresponding author E-mail: mhazizi@yahoo.com

including linear elasticity and plasticity. They are classic models which are founded on Von-Mises yield criterion, Drucker-Prager yield criterion and creep equations (Mohamed et al., 2009). Enomoto et al. (2015) simulated the creep behaviour of various viscous property types by the non-linear three-component model taking into account the effects of particle characteristics on the viscous property parameters. They concluded that the creep failure did not occur even under the nearly peak stress state in drained TC tests on air-dried Albany silica sand exhibiting P&N viscosity.

Methods which are based on Newton's laws, Bingham's laws or Norton's laws are generally suitable methods for simulating creep because they take the viscosity of materials into account (Vulliet and Hutter, 1998). However, elastovisco-plastic laws are very complex and do not generally follow physical rules. Jin et al. (2003) presented a Discrete Element Method (DEM) to simulate the creep behavior of jointed rock slopes resulting from unloading and excavation. They used Kelvin model to simulate viscose deformation of joints.

Yang et al. (2010) studied the creep behavior of frozen sands. They assessed a series of laboratory data under different stress levels at different temperatures. According to their results, the creep specification of frozen sand is highly affected by loading and temperature. Puzrin et al. (2012) studied a simple analytical model to evaluate the creep in a landslide stabilized by a retaining wall. Baba and Peth (2012) provided 2D-PIV analysis combined with large-scale box test to assess creep of different slopes. They showed that the micrometer-scale of soil motions is identifiable only through the natural texture of soil.

Zhou and Cheng (2015) developed a displacement-based LEM to analyze the stability and creep of slopes. They obtained the relation between shear displacement and creep time based on visco-elasoplastic creep model in the index point at crown. Camargo et al. (2016) proposed a numerical limit analysis to solve three-dimensional slope stability problems in large areas subjected to pore pressure effects.

Li et al. (2012) studied the optimal location of piles in slope stabilization by limit analysis. They obtained the factor of safety of piled slopes by the magnitude of resistive forces exerted by the piles on the slope. Yao et al. (2019) proposed a one-dimensional creep model that takes temperature as an independent variable for frozen soils. They established a novel model for directly describing the effect of the increase in temperature on the creep behavior of frozen soils.

Wang et al. (2019) analyzed the creep breakage mechanisms of frozen soils in detail by the concept of binary medium model under the framework of breakage mechanics for geomaterials. Venda Oliveira et al. (2019) analyzed the ability of the Singh-Mitchell and Taylor creep laws associated with a modified Cam clay model to predict the creep behavior of a soft soil subjected to preloading.

Aung et al. (2019) proposed a new mixed hardening hyper-viscoplasticity model for the derivation of the time-dependent constitutive behavior of soils, with the intention to capture the variation in the shapes of the yield loci by pursuing non-associated flow rules and accounting for kinematic hardening effects.

Wang et al. (2020) reported an in-situ direct shear creep test carried out in the shear zone of a reactivated slow-moving landslide in the TGR region. Correspondingly, some laboratory ring shear creep tests are carried out to interpret the movement pattern of this landslide. The shear zone soil exhibits similar non-attenuating creep responses in both the in-situ direct shear and laboratory ring shear creep tests. At the same stress level, however, the in-situ direct shear creep test yields a larger rate of creep displacement due to

shearing along the landslide direction. In the ring shear creep tests, at the prepeak stage, the critical creep stress that triggers creep failure is slightly lower than the peak shear strength but much larger than the residual strength; at the post failure stage, the critical creep stress of the shear-zone soil is equal to the residual shear strength. The rate-dependent residual shear strength may account for the stepwise movement pattern of the landslide. Feng et al. (2020) developed new simplified method to calculate the settlement of multi-layer soft soils exhibiting creep subjected to the multi-stage loading under a one-dimensional straining condition.

Determination of shear displacement value on critical slip surface is one of the importance issues to assess the stability status of an earth slope. There are several ways to determine the shear displacement that presents LEM for all slices in this study. In fact, this study presents a method for calculating time-dependent shear displacement during the creep of the failure surface of a slope in 2D static state for all slices of earth slope. To assess the creep of soil slope, the rheological behavior of soil is modeled using a series of springs and dashpots. Moment-force equilibrium equations are simultaneously satisfied to calculate shear displacement. This algorithm was developed in FORTRAN. Also, this method can be developed for 3D dimensional limit equilibrium (Hajiazizi, 2018), stabilization of earth slope (Hajiazizi, 2018), sliding slope (Hajiazizi, 2018) and soils under chemical corrosion (Wang et al., 2017)

HOW TO CALCULATE CREEP-INDUCED SLIP SURFACE DISPLACEMENT

Step 1:

Equilibrium equations are first obtained for all slices in both horizontal and vertical directions. Then, moment equilibrium equation is obtained. In addition, the assumption of the zero resultant for inter-slice forces should be met for all slices of failure surface. Shear stress is replaced in the equations based on Mohr-Coulomb criterion. The mentioned relations are simultaneously used to calculate the safety factor and the long-term shear stress for each slice.

Step 2:

Similar to step 1, force equilibrium equations are developed for all slices in both horizontal and vertical directions. Then, moment equilibrium equations are obtained. In addition, the assumption of zero resultant for inter-slice forces should be met for all slices of failure surface. The rheological behavior of soil is used and a series of differential equations are separately solved for elastic and plastic modes of soil in order to model the elasto-viscoplastic behavior of soil. Then, the displacement of the bottom of slice is obtained based on the displacement of the index point (at crown). The mentioned relations are simultaneously used in an iteration process and the time-dependent shear stress of soil, due to creep, is calculated using the safety factor and long-term shear stress relations calculated in the step 1.

Slope Creep Based on LEM

Forces Applied on Each Slice

Figure 1 shows the schematic view of forces applied on slice *i*. According to the figure, w_i: stands for the weight of slice *i*. In addition, N_i and S_i: stand for normal and shear forces acting on slip surface. Q_{i-1} and Q_i: indicate the inter-slice force between slices *i* and *i-1* and the inter-slice force between slices *i* and *i+1*, respectively. α_i and β: indicate the inclination angle of the base of slice *i* and the angle orientation of the inter-slice forces, respectively.

Equilibrium Equations

In Figure 1, the difference of inter-slice force is written as $\Delta Q_i=Q_i-Q_{i-1}$. Force

equilibrium equations in x and y-axes are as follows:

$$\sum F_x = 0 \implies -N_i \ sin\,\alpha_i + S_i \ cos\,\alpha_i + \Delta Q_i \ cos\,\beta = 0 \quad (1)$$

$$\sum F_y = 0 \implies N_i \ cos\,\alpha_i + S_i \ sin\,\alpha_i + \Delta Q_i \ sin\,\beta - W_i = 0 \quad (2)$$

The boundary conditions of intersegment force are Q_0=0 and Q_n=0. The moment of inter-slice forces around the axes is zero. Moment equilibrium equations around point z are written as follows:

$$\sum_n M_z = 0 \implies \sum_{i=1} (N_i \ cos\,\alpha_i + S_i \ sin\,\alpha_i) \ x_i + (N_i \ sin\,\alpha_i - S_i \ cos\,\alpha_i) \ y_i - W_i \ x_i = 0 \quad (3)$$

where x_i and y_i: are distance to point z.

The force equilibrium equation is $\sum \Delta Q_i = 0$ where ΔQ_i: is the resultant of inter-slice force.

$$\sum \Delta Q_i = 0 \quad (4)$$

By combining Eqs. (1) and (2) we have:

$$N_i \ cos(\alpha_i - \beta) + S_i \ sin(\alpha_i - \beta) - W_i \cos\beta = 0 \quad (5)$$

in the first step, S^i_{long} and safety factor using Spencer method are calculated as follows; where S^i_{long} is long-term shear strength and will be discussed later.

According to Mohr-Coulomb criterion we have:

$$S_i = \frac{N \ tan\,\varphi + C}{RF} \quad (6)$$

$$C = c \ l_i \quad (7)$$

where *RF*: is the reduction factor for LE. φ' and c': are the effective internal friction angle and cohesion of the slope materials, respectively. l_i: is the length of slice i.

By replacing Eq. (6) in Eq. (5) we have:

$$N_i = \frac{RF \ W_i \ cos\,\beta - c \ l_i \ sin(\alpha_i - \beta)}{RF \ cos(\alpha_i - \beta) + tan\,\varphi \ sin(\alpha_i - \beta)} \quad (8)$$

and,

$$S_i = \frac{W_i \cos\beta \ tan\,\varphi + c \ l_i \ cos(\alpha_i - \beta)}{RF \ cos(\alpha_i - \beta) + tan\,\varphi \ sin(\alpha_i - \beta)} \quad (9)$$

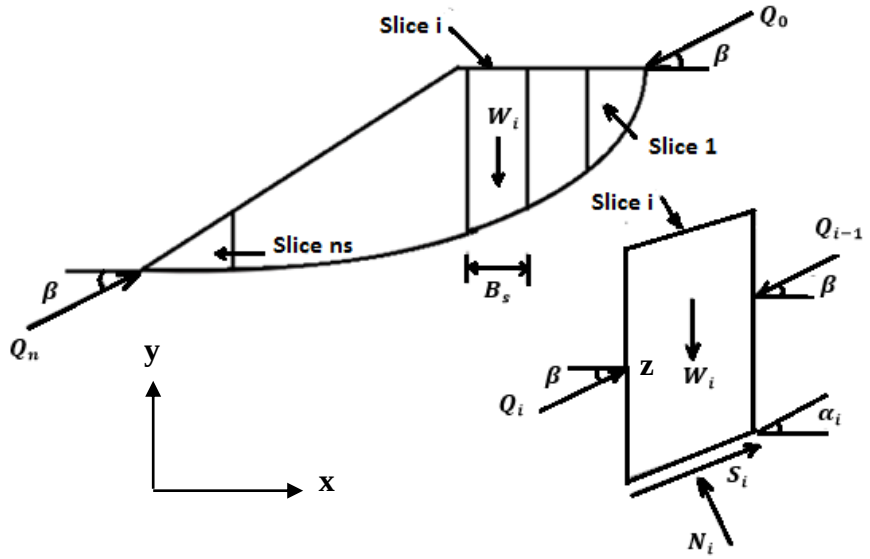

Fig. 1. Diagram of forces that act on the slice i of a non-circular sliding surface

Then, by replacing Eqs. (8) and (9) in moment equilibrium equation (Eq. (3)) and force equilibrium equation (Eq. (4)), the following equations are derived:

$$F_z(\beta, RF) = \sum M_z = 0 \quad (10)$$

and,

$$F_x(\beta, RF) = \sum F_x = 0 \quad (11)$$

By the simultaneous solution of Eqs. (10-11) and determining β, RF and replacing them in Eq. (9), the value of S_i is obtained. Then, S_{long}^{i} is calculated using Eq. (12).

$$S_{long}^{i} = \lambda_i S_i \quad (12)$$

or,

$$\tau_{long}^{i} = \lambda_i \tau_f^{i} = \lambda_i \frac{\sigma'_{nl} tan\,\varphi + c}{RF} \quad (13)$$

where τ_{long}^{i}: is the long-term yield stress.

$$S_{long}^{i} = \tau_{long}^{i} l_i \quad (14)$$

Displacement-Based Visco-Elastoplastic Relations

Basic Formulas of Visco-Elastoplastic Model

Visco-elastoplastic creep model consists of three parts, body hook (H), body visco-elastic and body visco-plastic connected to each other in series.

In this model, G_1, G_2, η_1, η_2 and τ_{long}^{i}: stand for the shear module of body hook, the shear modulus of viscoelastic body, the viscosity coefficient of viscoelastic body, the viscosity coefficient of viscoplastic body and the yield strength of viscoplastic body, which is called long-term shear strength, respectively. When shear stress,(τ_i) is lower than yield stress,τ_{long}^{i} viscoelastic creep deformation occurs in the soil. In contrast, when shear stress,(τ_i) is higher than yield stress,τ_{long}^{i} viscoealstoplastic deformation occurs in the soil. Long-term shear stress τ_{long}^{i} is associated with instant shear strength. In general, it is defined by Mohr-Coulomb failure criterion. Table 1 shows long-term shear strength to instant shear strength ratio,$\left(\lambda_i = \tau_{long}^{i}/\tau_i\right)$, based on laboratory results (Zhou and Cheng, 2015).

When slip wedge starts moving, Mohr-Coulomb failure criterion is satisfied. Therefore, long-term shear stress, τ_{long}^{i}, can be derived from the following relation:

$$\tau_{long}^{i} = \lambda_i \tau_f^{i} = \lambda_i \frac{\sigma'_{nl} tan\,\varphi + c}{RF} \quad (15)$$

where τ_f^{i}: is the instant shear strength of soil based on Mohr-Coulomb failure criterion and σ'_{nl}: is the normal stress acting on the base of the slice i.

The long-term shear strength of slice force i, S_{long}^{i}, is derived from the following relation (Zhou and Cheng, 2015):

$$S_{long}^{i} = \tau_{long}^{i} l_i \quad (16)$$

The constitutive model of visco-elastoplastic is obtained as follows:

- When shear stress, (τ^i), is lower than yield stress, τ_{long}^{i}, the relation between shear stress and shear strain is as follows:

$$\frac{\eta_1}{G_1 + G_2}\dot{\tau}^i + \tau^i = \frac{G_1\eta_1}{G_1 + G_2}\dot{\gamma}^i + \frac{G_1 G_2}{G_1 + G_2}\gamma^i \quad (17)$$

where $\dot{\tau}^i = d\tau^i/dt$ and $\dot{\gamma}^i = d\gamma^i/dt$ and γ: is shear strain.

- When shear stress, (τ^i), is higher than yield stress, τ_{long}^{i}, the relation between shear stress and shear strain is as follows:

Table 1. The ratio of the long-term shear strength and the instantaneous shear strength of some geomaterials (Zhou and Cheng, 2015)

Geomaterials	Clay soil	Limestone	Salina stone	Sand stone	Chalk	Clay shale
λ_i	0.74	0.73	0.70	0.65	0.62	0.50

$$\ddot{\tau}^i + \left(\frac{G_1}{\eta_1} + \frac{G_2}{\eta_2} + \frac{G_2}{\eta_1}\right)\dot{\tau}^i + \frac{G_1\,G_2}{\eta_1\eta_2}\left(\tau^i - \tau^i_{long}\right) = G_1\,\ddot{\gamma}^i + \frac{G_1 G_2}{\eta_1}\dot{\gamma}^i \tag{18}$$

where $\ddot{\tau}^i = d^2\tau^i/dt^2$ and $\ddot{\gamma}^i = d^2\gamma^i/dt^2$. These relations are differential equations of order two to obtain shear stress and shear strain.

Shear stress-strain relation can be converted to shear force-displacement relation in accordance with the following relation:

$$\gamma^i = \frac{\Delta^i_{shear}}{l_i} \tag{19}$$

$$\tau^i = \frac{S^i}{l_i} \tag{20}$$

When Shear Force Is Lower Than Long-Term Shear Strength

When shear force, (S^i), which acts on the bottom of slice *i*, is lower than long-term shear strength, shear force-displacement relation corresponding to Eq. (17) will be derived as follows:

$$\frac{G_1\eta_1}{G_1+G_2}\,\frac{d\Delta^i_{shear}(t)}{dt} + \frac{G_1\,G_2}{G_1+G_2}\,\Delta^i_{shear}(t) = \frac{\eta_1}{G_1+G_2}\frac{dS^i}{dt} + S^i \tag{21}$$

where $\Delta^i_{shear}(t)$, S^i and t: are the shear displacement of slice *i*, the shear stress of the bottom of slice *i* and creep time, respectively. S^i does not vary with time. Therefore, $\frac{dS^i}{dt} = 0$. Considering the fact that the initial shear displacement is $\frac{S^i}{G_1}$, i.e. $\Delta^i_{shear}(0) = \frac{S^i}{G_1}$, the differential Eq. (21) is solved as follows:

$$\frac{G_1\eta_1}{G_1+G_2}\,\frac{d\Delta^i_{shear}(t)}{dt} + \frac{G_1\,G_2}{G_1+G_2}\,\Delta^i_{shear}(t) = S^i \tag{22}$$

With multiplying in $\frac{G_1+G_2}{G_1G_2}$,

$$\frac{\eta_1}{G_2}\,\frac{d\Delta^i_{shear}(t)}{dt} + \Delta^i_{shear}(t) = \frac{G_1+G_2}{G_1\,G_2}S^i \tag{23}$$

Shear displacement is:

$$\Delta^i_{shear}(t) = y \tag{24}$$

Derivative of shear displacement is:

$$\frac{d\Delta^i_{shear}(t)}{dt} = \dot{y} \tag{25}$$

Eq. (23) can be rewritten as follows:

$$\frac{\eta_1}{G_2}\,\dot{y} + y = \frac{G_1+G_2}{G_1\,G_2}S^i \tag{26}$$

By arranging the Eq. (26),

$$\dot{y} + \frac{G_2}{\eta_1}\,y = \frac{G_1+G_2}{G_1\,G_2}\,\frac{G_2}{\eta_1}\,S^i \tag{27}$$

The solution of the second-order differential equation Eq. (27) is as follows:

$$y = e^{-\int\frac{G_2}{\eta_1}dt}\left[\int\left(\frac{G_1+G_2}{G_1\,G_2}\,\frac{G_2}{\eta_1}\,S^i\right)e^{\int\frac{G_2}{\eta_1}dt}\,dt + c\right] \tag{28}$$

$$y = e^{-\frac{G_2}{\eta_1}t}\left[\int\left(\frac{G_1+G_2}{G_1\,G_2}\,\frac{G_2}{\eta_1}\,S^i\right)e^{\frac{G_2}{\eta_1}t}\,dt + c\right] \tag{29}$$

or,

$$y = e^{-\frac{G_2}{\eta_1}t}\left[\left(\frac{G_1+G_2}{G_1\,G_2}\,\frac{G_2}{\eta_1}\,S^i\right)\frac{\eta_1}{G_2}e^{\frac{G_2}{\eta_1}t}+c\right] \tag{30}$$

or,

$$y = \frac{G_1+G_2}{G_1\,G_2}\,S^i + c\,e^{-\frac{G_2}{\eta_1}t} \tag{31}$$

Therefore, the shear displacement is obtained from the Eq. (32).

$$\Delta^i_{shear}(t) = \frac{G_1+G_2}{G_1\,G_2}\,S^i + c\,e^{-\frac{G_2}{\eta_1}t} \qquad S^i < S^i_{long} \tag{32}$$

Initial Condition

Initial condition of $\Delta^i_{shear}(0) = \frac{S^i}{G_1}$ for calculating *c* is:

$$c = \frac{S^i}{G_1} - \frac{G_1+G_2}{G_1\,G_2}\,S^i \tag{33}$$

Then shear displacement is obtained as follows:

$$\Delta^i_{shear}(t) = \frac{S^i}{G_1} + \frac{S^i}{G_2}\left(1-e^{-\frac{G_2}{\eta_1}t}\right) \qquad for\ S^i < S^i_{long} \tag{34}$$

When Shear Force Is Higher Than Long-Term Shear Strength

When shear force, acting on the bottom of slice *i* is higher than long-term shear strength, shear force-displacement relation corresponding to Eq. (18) will be as follows:

$$G_1\frac{d^2\Delta^i_{shear}(t)}{dt^2} + \frac{G_1G_2}{\eta_1}\frac{d\Delta^i_{shear}(t)}{dt} = \frac{d^2S^i}{dt^2} + \left(\frac{G_1}{\eta_1}+\frac{G_2}{\eta_2}+\frac{G_2}{\eta_1}\right)\frac{dS^i}{dt} + \frac{G_1\,G_2}{\eta_1\,\eta_2}\left(S^i - S^i_{long}\right) \tag{35}$$

where S^i: does not vary with time. Therefore, $\frac{dS^i}{dt} = 0$. Considering the fact that the initial shear displacement is $\frac{S^i}{G_1}$, i.e. $\Delta^i_{shear}(0) = \frac{S^i}{G_1}$, and considering that creep-shear displacement of soil exponentially vary with time until the completion of the first creep time (t_1), the equation for calculating shear displacement will follow Eq. (35). After t_1, shear displacements enters to the second step where creep linearly increases with time.

If the displacements are small enough to prevent the third stage creep, the curve of displacement due to creep-time will be approximately the same as the continuous line. According to Bingham's equation, the slope of creep line is $\frac{\left(S^i - S^i_{long}\right)}{\eta}$. In visco-elastoplastic creep, the linear part of creep, i.e. the second step, equals to the dashpot (η_2) and plastic slider (G_2) connected to each other in parallel and is related to other sets in series. Therefore, the second step of creep is a straight line with a slope of $\frac{\left(S^i - S^i_{long}\right)}{\eta_2}$ and the creep for $S^i > S^i_{long}$ mode is calculated as follows:

$$G_1\frac{d^2\Delta^i_{shear}(t)}{dt^2} + \frac{G_1G_2}{\eta_1}\frac{d\Delta^i_{shear}(t)}{dt} = \frac{G_1\,G_2}{\eta_1\,\eta_2}\left(S^i - S^i_{long}\right) \tag{36}$$

Therefore, the shear displacement is obtained from the Eq. (37) for $S^i > S^i_{long}$,

$$\Delta^i_{shear}(t) = \frac{S^i}{G_1} + \frac{S^i}{G_2}\left(1-e^{-\frac{G_2}{\eta_1}t}\right) + \frac{\left(S^i - S^i_{long}\right)}{\eta_2}t \qquad S^i > S^i_{long} \tag{37}$$

Therefore, Eqs. (34) and (37) are the relations between shear force and shear displacement in visco-elastoplastic creep

model under shear stress.

Displacement Compatibility between Slices

By using the displacement vectors and displacement compatibility between slices can write:

$$\Delta_i = \Delta_0 \,.\, f(\alpha_i) \tag{38}$$

where

$$f(\alpha_i) = \frac{1}{sin(\alpha_1 - \psi)} \,.\, \frac{cos(\alpha_1 - 2\psi)}{cos(2\psi - \alpha_i)} \tag{39}$$

where ψ: is dilation angle.

When shear force (S^i) is lower than long-term shear strength, $\left(S^i_{long}\right)$, the relation between shear force and vertical displacement in the index point at crown, of the first slice will be as follows:

$$\Delta_0(t) = \frac{K_1}{f(\alpha_i)}\, S^i \quad S^i < S^i_{long} \tag{40}$$

where

$$K_1 = \frac{1}{G_1} + \frac{1}{G_2}\left(1 - e^{-\frac{G_2}{\eta_1}t}\right) \quad S^i < S^i_{long} \tag{41}$$

and

$$f(\alpha_i) = \frac{1}{sin(\alpha_1 - \psi)} \,.\, \frac{cos(\alpha_1 - 2\psi)}{cos(2\psi - \alpha_i)} \quad S^i < S^i_{long} \tag{42}$$

and

$$S^i = \frac{\Delta_0(t)\, f(\alpha_i)}{K_1} \qquad S^i < S^i_{long} \tag{43}$$

By replacing Eq. (48) in Eq. (19), normal force is obtained as follows:

$$N_i = \frac{W_i \cos\beta}{cos(\alpha_i - \beta)} - \frac{\Delta_0(t)\, f(\alpha_i)}{K_1} tan(\alpha_i - \beta) \tag{44}$$

when shear force (S^i) is higher than long-term shear strength, $\left(S^i_{long}\right)$. The relation between shear force and vertical displacement in the index point is obtained as follows:

$$\Delta_0(t) = \frac{1}{f(\alpha_i)}\left(K_1 S^i + K_2 (S^i - S^i_{long})\right) \quad S^i > S^i_{long} \tag{45}$$

where

$$K_2 = \frac{t}{\eta_2} \quad S^i > S^i_{long} \tag{46}$$

and

$$S^i = \frac{\Delta_0(t)\, f(\alpha_i) + K_2 S^i_{long}}{K_1 + K_2} \quad S^i > S^i_{long} \tag{47}$$

By replacing Eq. (47) in Eq. (14), normal force will be obtained as follows:

$$N_i = \frac{W_i \cos\beta}{cos(\alpha_i - \beta)} - \left(\frac{\Delta_0(t)\, f(\alpha_i) + K_2 S^i_{long}}{K_1 + K_2}\right) tan(\alpha_i - \beta) \tag{48}$$

By replacing Eqs. (43, 44, 47 and 48) in moment equilibrium equation (Eq. (3)) and force equilibrium equation (Eq. (4)), the following equations are derived:

$$M_z(\beta, \Delta_0(t), t) = \sum M_z = 0 \tag{49}$$

$$F_x(\beta, \Delta_0(t), t) = \sum F_x = 0 \tag{50}$$

The simultaneous solution of the above equations yields $\Delta_0(t)$, β for different times. An initial β(=0) is first assumed in moment equilibrium equation and an initial $\Delta_0(t)$ is obtained for the arbitrary time t. Then, β and $\Delta_0(t)$ are replaced in force equilibrium

equation. If the force equilibrium equation is satisfied for the initial β and $\Delta_0(t)$, they will be considered as the solutions of the equation otherwise, $\beta+\Delta x$ is replaced with the initial β and this is repeated until both moment and force equilibrium equations are simultaneously satisfied for a suitable β and $\Delta_0(t)$.

Then, the creep-induced shear displacement of slice *i* on the slip surface is derived from the following relation:

$$\Delta_{shear}^{i}(t) = \Delta_0(t) \,.\, f(\alpha_i) \qquad (51)$$

The algorithm is coded in Fortran on the flowchart shown in Figure 2.

NUMERICAL MODELING

In this paper, numerical modeling was carried out using 2D finite difference method. Global and local mesh refinements defined to certify a good quality of the mesh. The finite difference method was used for the numerical modeling with rectangular mesh. Based on sensitive analysis performed for two examples, number of elements is 2655. Mohr-Coulomb criterion is considered as behavior model. In numerical models, static condition were considered for boundary condition of each models, in which, sides boundaries were fixed along x, and the bottom boundary was fixed along x and y axes.

EXAMPLES

To examine the proposed method for viscoelastic and visco-elstoplastic analysis, two practical examples are presented in this paper. An earth slope with simple geometry is considered in first example. To illustrate the ability of the proposed method in earth slope with safety factor lesser than 1, is considered in second example. In these examples, the results of proposed method are compared with those obtained from FEM. It is worth noting that the considered examples are solved by a computer code written using Fortran software.

Example 1:

In this example a slope with a height of 20 m is studied (slope angle=45^o) and the number of slices is 150. Table 2 shows the specifications of the slope. If the shear stress in each slice is lower than the long-term shear strength of soil, or in other words, if the safety factor of slope > 1, the creep of the slope will be in elastic mode and the relations of viscoelastic rheological behavior are used. If the shear stress in each slice is higher than the long-term shear strength of soil, or in other words, if the safety factor of slope < 1, the creep of the slope will be in plastic mode and the relations of visco-elastoplastic rheological behavior are used to calculate the creep of soil.

In this example, the safety factor is 1.49 and the slope is stable and shows viscoelastic creep behavior. Figure 3 shows the viscoelastic vertical displacement versus creep time at crown using the proposed method using proposed method and FEM which are consistent with each other. In this figure after t=10000000 the vertical displacement remains constant and maximum vertical displacement is about 2.8 cm. Figure 4 shows viscoelastic shear displacement versus creep time along the slip surface for different slices. As the number of slices increase, shear displacements converge. As the number of slices increases more precise shear displacement will be achieved.

Table 2. The specifications of the modeled slope

E	C	Ø	v	γ_d
1118 MPa	55 kPa	26	0.3	24.92 kN/m^3

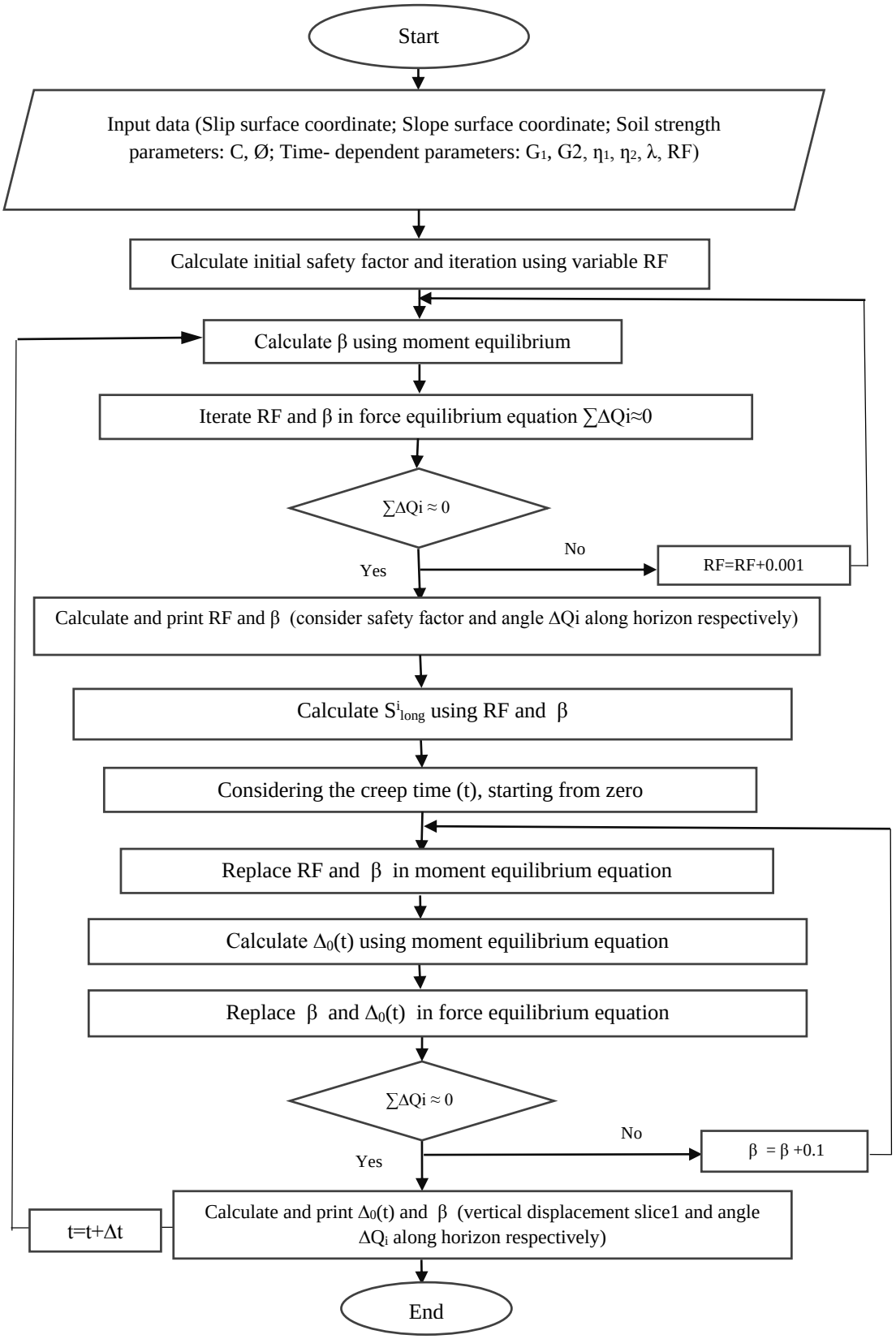

Fig. 2. Flowchart calculated vertical displacement of the crown and shear displacement with time of creep at bottom slices on the surface of the slope failure due to gravity load

This problem has been also solved using Finite Element Method (FEM). Shear displacement on the slip surface when displacement with time converges to a constant value is shown in Figure 5. Examining this figure, it is verified that the obtained shear displacements in the crown and the toe of slope are in good agreement with those obtained using FEM. However, it should be noted that the good agreement in other slices are less. The obtained shape using proposed method is similar to slip surface of slope whereas the obtained shape using FEM is about linear. It seems that the shape of the proposed method has a better description of the shear displacement on the slip surface than the FEM.

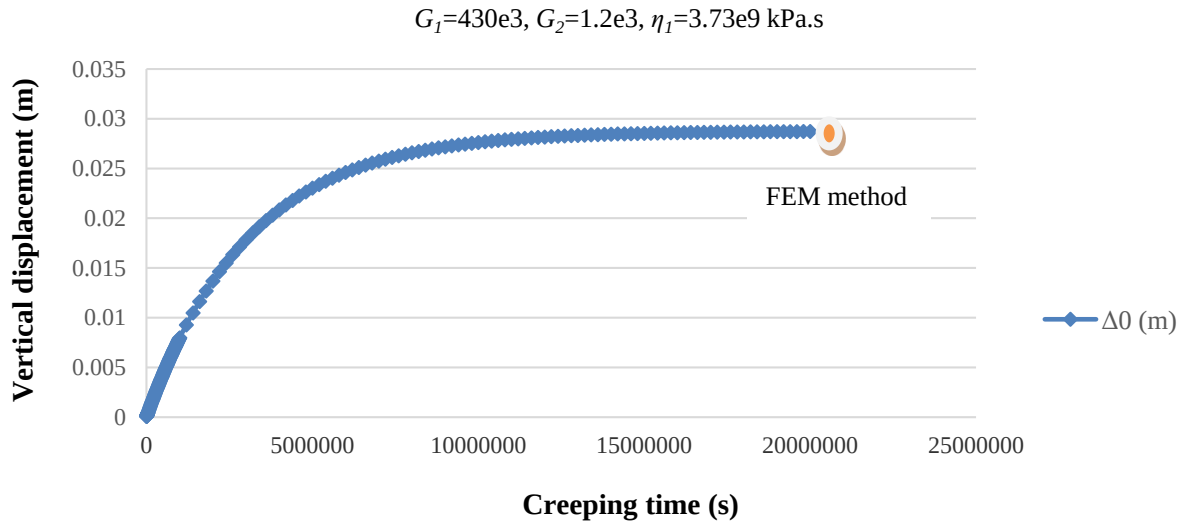

Fig. 3. Vertical displacement of viscoelastic on the crown of the slope with creeping time using the proposed method and FEM which are consistent with each other

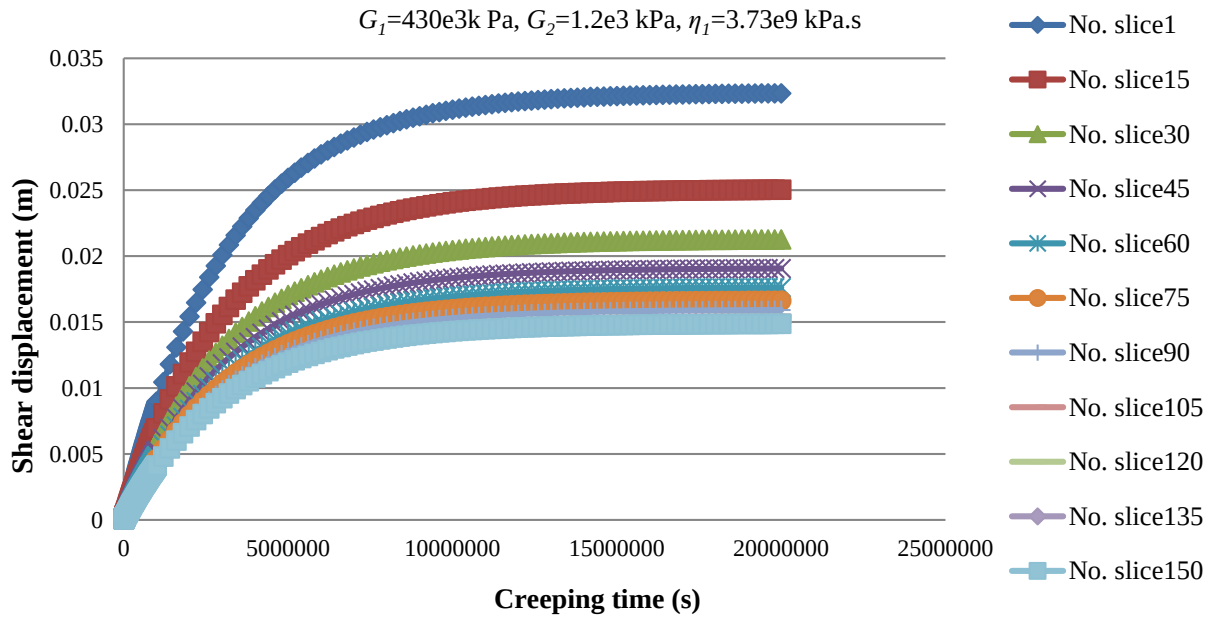

Fig. 4. Shear displacement of viscoelastic on the slip surface with creeping time using the proposed method for different slices

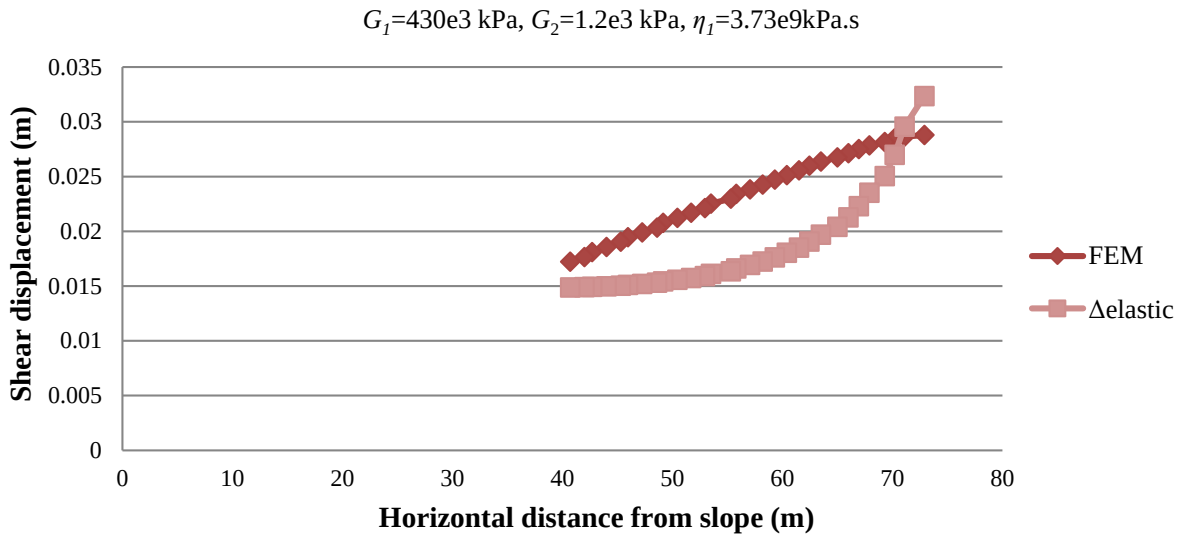

Fig. 5. Shear displacement on the slip surface when displacement with time converges to a constant value using proposed method and FEM

The Effect of G_2 and η_1 Parameters on Viscoealstic Shear Displacement versus Creep Time

G_2 Variations

Figure 6 shows viscoelastic vertical displacement versus creep time at the crown of the slope of Example 1 where G_2 changes and other parameters remain constant. According to the curve, as G_2 increases, vertical displacement decreases.

η_1 Variations

Figure 7 shows viscoelastic vertical displacement versus creep time at crown where η_1 changes and other parameters remain constant. As η_1 increases, vertical displacement decreases. The best fit with conventional creep curves is achieved for η_1=3.73e9 kPa.s and smaller values. As η_1 decreases, vertical displacement curve shifts left side implying that the soil reaches its final creep within a shorter time.

Example 2

This example studies a soil slope with a height of 20 m and the number of slices is 150 and the slope angle is 45º. Table 3 shows the specifications of the slope.

In this example, the minimum safety factor is 0.42 and the slope is instable and shows visco-elastoplastic creep behavior. Figure 8 shows vertical displacement versus creep time at the crown of the slope using the proposed method. As seen, variations of viscoelastic are constant, while variations of visco-elastoplastic are increasing. Figure 9 shows visco-elastoplastic shear displacement versus creep time along the failure surface over time. As the number of slices increase, shear displacements converge.

This problem has been also solved using FEM. Shear displacement on the slip surface when displacement with time converges to a constant value is shown in Figure 10. Examining this figure, it is verified that the obtained shear displacements in the crown and the toe of slope are in good agreement with those obtained using FEM. However, it should be noted that the good agreement in other slices are less. The obtained shape using proposed method is similar to slip surface of slope whereas the obtained shape using FEM is about linear. It seems that the shape of the proposed method has a better description of the shear displacement on the slip surface than the FEM.

Table 3. The specifications of the modeled slope

E	C	Ø	v	γ_d
91 MPa	10 kPa	10	0.3	24.92 kN/m^3

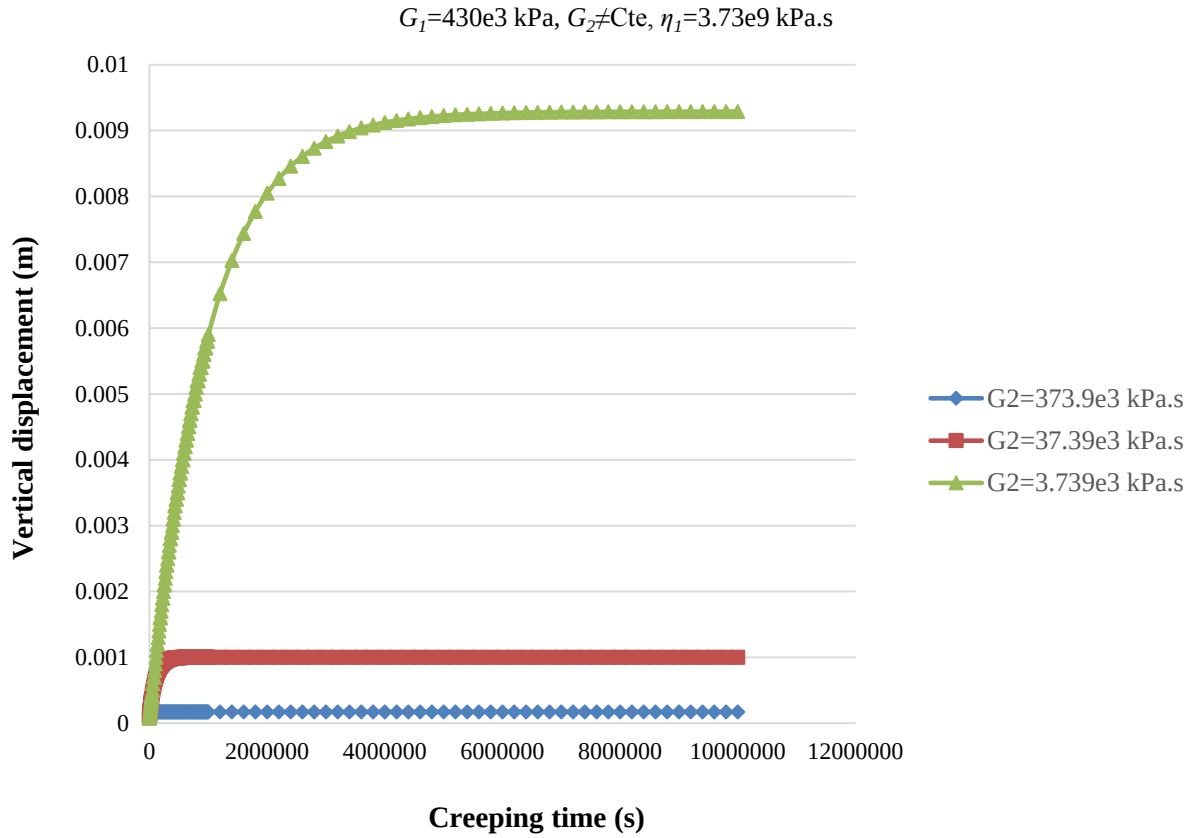

Fig. 6. Vertical displacement of viscoelastic on the crown of the slope with creeping time for changing parameter of G_2 and fixing other parameters using the proposed method

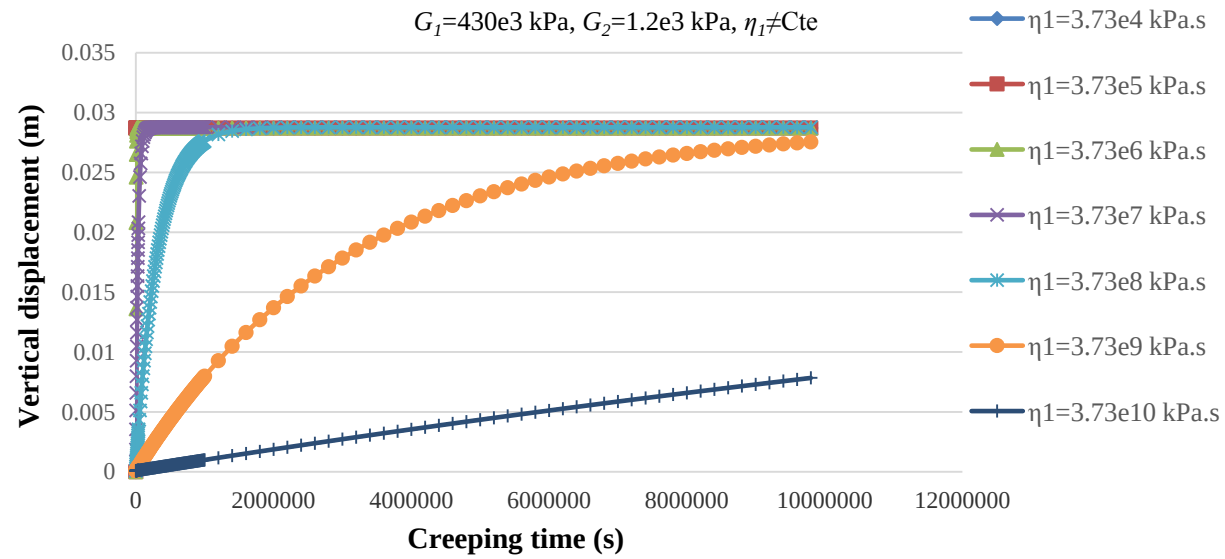

Fig. 7. Vertical displacement of viscoelastic on the crown of the slope with creeping time for changing parameter of η_1 and fixing other parameters using the proposed method

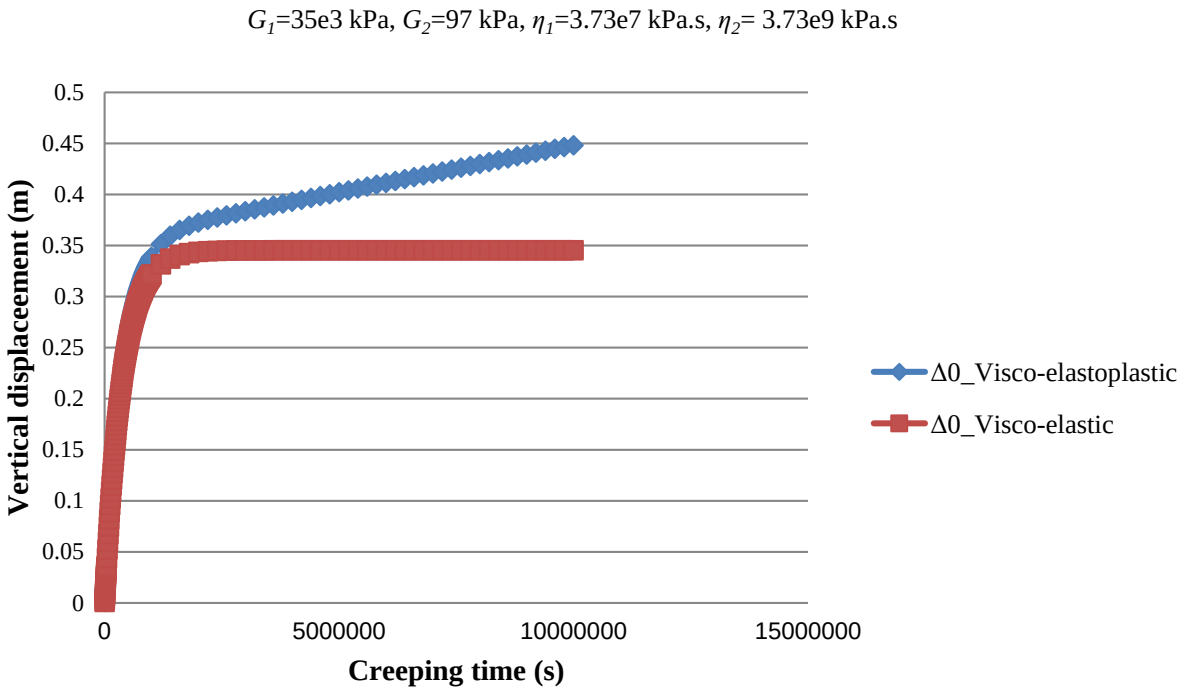

Fig. 8. Vertical displacement of visco-elastic and visco-elastoplastic on the crown of the slope with creeping time using the proposed method for visco-elastic and visco-elastoplastic

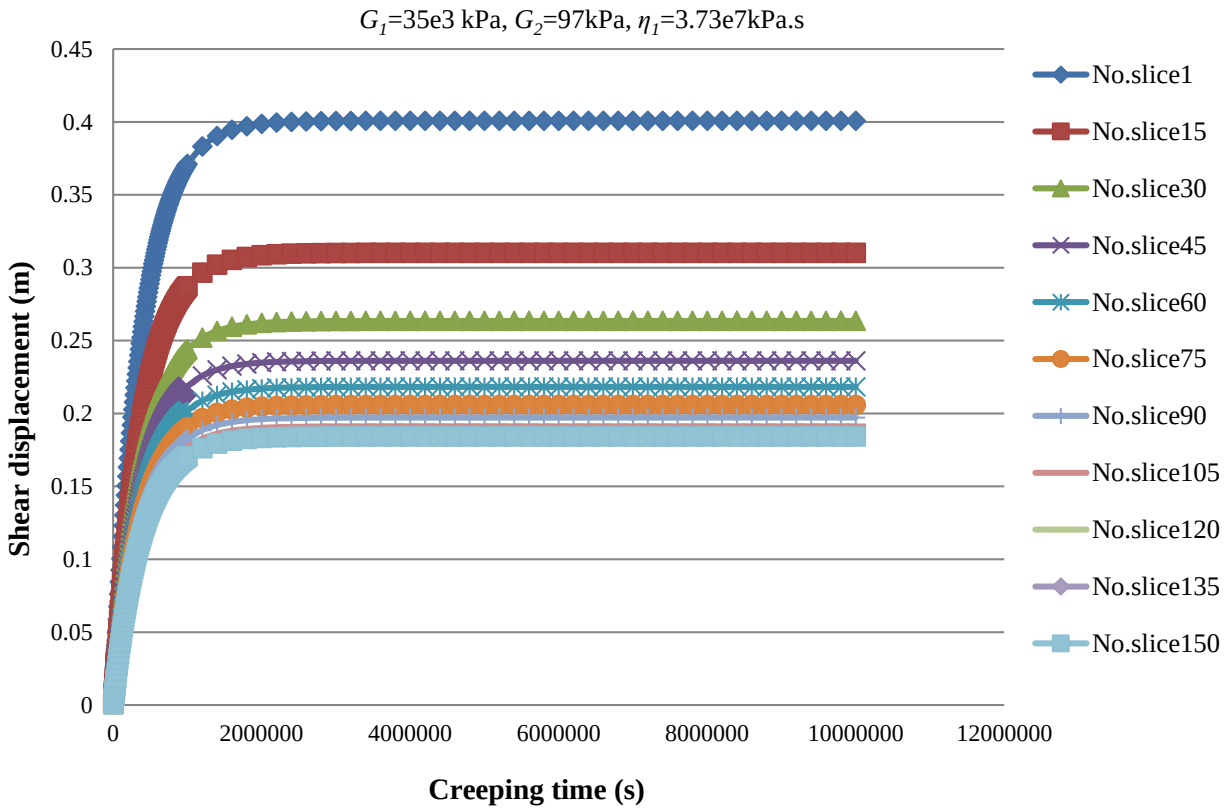

Fig. 9. Shear displacement of visco-elastoplastic points on the surface sliding with creeping time using the proposed method for different slices

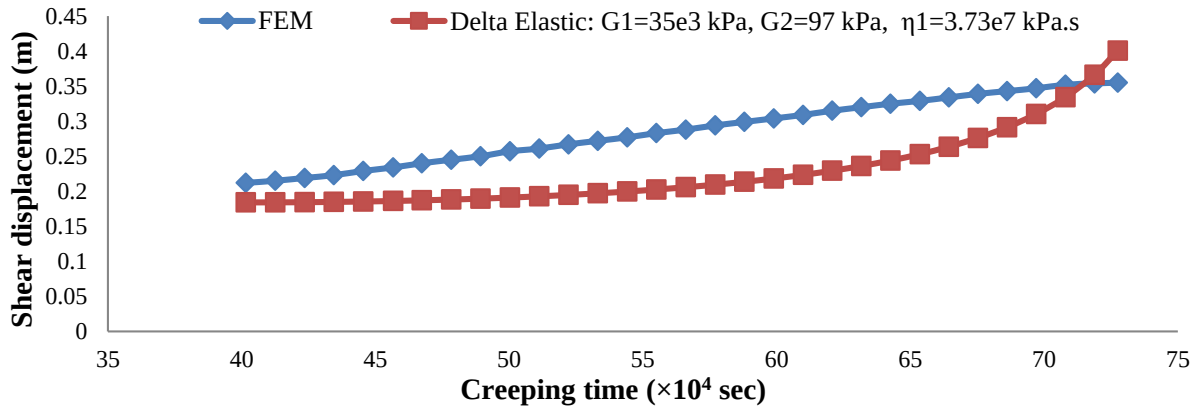

Fig. 10. Shear displacement on the slip surface when displacement with time converges to a constant value using the proposed method and FEM

Effects of G_2, η_1 and η_2 on Visco-elastoplastic Shear Displacement Versus Creep Time

G_2 Variations

Visco-elastoplastic shear displacement versus creep time at crown studied where G_2 changes and other parameters remain constant. As G_2 increases, viscoplastic shear displacement decreases.

η_1 Variations

Visco-elastoplastic shear displacement versus creep time at crown studied where η_1 changes and other parameters remain constant. As η_1 increases, visco-elastoplastic shear displacement decreases. In addition, the curve well fits with conventional creep curves for η_1=3.73e8 kPa.s, and smaller values and the best fit is achieved for η_1=3.73e7 kPa.s. As η_1 decreases, the soil reaches its final creep displacement within a shorter time.

η_2 Variations

Figure 11 shows visco-elastoplastic shear displacement versus creep time where η_2 changes and other parameters remain constant. As η_2 increases, visco-elastoplastic shear displacement decreases. The secondary creep increases for η_2=3.73e9 kPa.s, and smaller values. However, for η_2>3.73e9 kPa.s, displacement remains constant.

Example 3

According to Zhou and Cheng (2015) the following parameters for the creep model are listed as follows: G_1=35×106 Pa, G_2=40×106 Pa, η_1=3.73×1012 Pa·s and η_2=3.73×1012 Pa·s. They founded that the long-term factor of safety of the 3D creeping slope is 0.42. The vertical displacements at the key point can be determined using the proposed method, as shown in Figure 12 (Zhou and Cheng, 2015).

It is found from this figure that the vertical displacement at the key point increases with increasing the creep time when the reduction factor is constant, while the vertical displacement at the key point converges to a constant value when the creep time exceeds a certain value. The long-term vertical displacements at the key point Δ_0 are respectively equal to 0.1064 m, 0.12422 m, 0.15628 m, 0.19165 m, 0.23885 m, 0.2909 m, 0.372 m, 0.54257 m and 0.7892 m when the reduction factors Δ_0 are 0.36, 0.37, 0.38, 0.39, 0.40, 0.41, 0.42, 0.43 and 0.44. The relationship between the long-term vertical displacement at the key point and the reduction factor is plotted in Figure 13 (Zhou and Cheng, 2015). It is found that the long-term vertical displacement at the key point sharply increases when the reduction factor exceeds 0.42. The results show that the key point displacement is 0.372 m that it is close to Zhou and Cheng (2015) result.

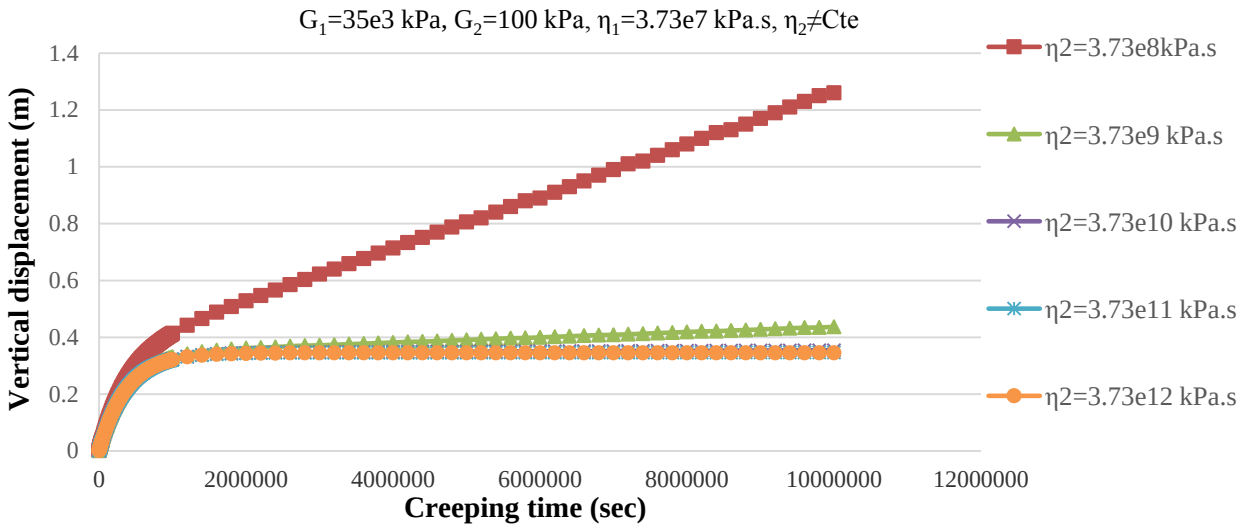

Fig. 11. Vertical displacement of visco-elastoplastic on the crown of the slope with creeping time for changing parameter of η_2 and fixing other parameters using the proposed method

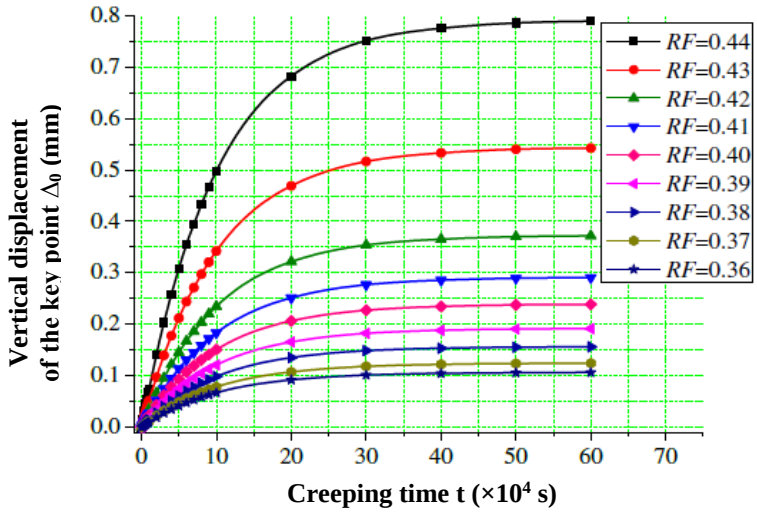

Fig. 12. Vertical displacement at the key point for various RF (Zhou and Cheng, 2015)

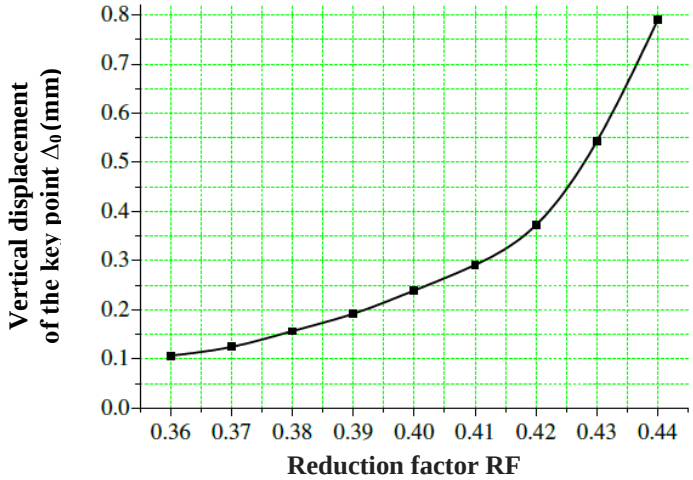

Fig. 13. Long term vertical displacement with various RF (Zhou and Cheng, 2015)

DISCUSSION

The relation between shear displacement and creep time is obtained based on visco-elastoplastic creep model. If the shear stress in each slice is lower than the long-term shear strength of soil, or in other words, if the safety factor of slope > 1, the creep of the slope will be in elastic mode and the relations of viscoelastic rheological behavior are used. If the shear stress in each slice is higher than the long-term shear strength of soil, or in other words, if the safety factor of slope < 1, the creep of the slope will be in plastic mode and the relations of visco-elastoplastic rheological behavior are used to calculate the creep of soil.

Figures 3, 5 and 10 show the displacement using the proposed method and FEM which are consistent with each other. If the shear stress in each slice is higher than the long-term shear strength of soil, the creep of the slope will be in plastic mode and the relations of visco-elastoplastic rheological behavior are used to calculate the creep of soil and reasonable results are obtained.

SUMMARY AND CONCLUSION

This paper provided a novel LEM-based analytical approach for all slices to calculate the elastic and the creep displacement of slopes. In the proposed approach, force and moment equilibrium equations are simultaneously satisfied. The relation between shear displacement of slope and creep time was obtained based on visco-elastoplastic creep model. A general safety factor was first derived for failure surface using Spencer method. Then, the shear displacement of all slices was obtained in terms of the vertical displacement of the index point at slope crown using the relation allocated for slope displacement and considering displacement compatibility between slices. There are several results which are considering:

- The results of the proposed method and FEM for the obtained shear displacements in the crown and the toe of slope are in excellent agreement.
- The elastic and the creep displacement of slopes for all slices were calculated using LEM-based analytical approach and FEM which reasonable and good agreement results are obtained.
- The time-dependent shear stress of soil, due to creep was calculated using the safety factor and reasonable results are obtained.
- If the shear stress in each slice is lower than the long-term shear strength of soil, the creep of the slope will be in elastic mode and the relations of visco-elastic rheological behavior are used for calculating the displacement of each slice and reasonable results are obtained.
- If the shear stress in each slice is higher than the long-term shear strength of soil, the creep of the slope will be in plastic mode and the relations of visco-elastoplastic rheological behavior are used to calculate the creep of soil and reasonable results are obtained.
- As G_2 increases, slope displacement decreases.
- As η_1 decreases, the soil reaches its final creep within a shorter time.
- As η_2 decreases, creep increases and η_2 affects visco-elastoplastic displacement and it can be argued that it affects the secondary creep of soil.
- The method in this paper has a theoretical significance and can be extended in the other applications.

REFERENCES

Augustesen, A., Liingaard, M. and Lade, P.V. (2004). "Evaluation of time-dependent behavior of soils", *International Journal of Geomechanics*, 4(3), 137-156.

Aung, Y., Khabbaz, H. and Fatahi, B. (2019). "Mixed hardening hyper-viscoplasticity model for soils incorporating non-linear creep rate, H-creep model", *International Journal of Plasticity*, 120, 88-114.

Baba, H.O. and Peth, S. (2012). "Large scale soil box test to investigate soil deformation and creep movement on slopes by Particle Image Velocimetry (PIV)", *Soil and Tillage Research*, 125, 38-43.

Camargo, J., Velloso, R.Q. and Vargas, E.A. (2016). "Numerical limit analysis of three-dimensional slope stability problems in catchment areas", *Acta Geotechnica*, 11(6), 253-259.

Enomoto, T., Koseki, J., Tatsuoka, F. and Sato, T. (2015). "Creep failure of sands exhibiting various viscosity types and its simulation", *Soils and Foundations*, 55(6), 1346-1363.

Feng, W., Yin, J., Chen, W., Tan, D. and Wu, P. (2020). "A new simplified method for calculating consolidation settlement of multilayer soft soils with creep under multi-stage ramp loading", *Engineering Geology*, 264, 105322.

Jin, F., Zhang, C.H., Wang, G. and Wang, G.L. (2003). "Creep modeling in excavation analysis of a high rock slope", *Journal of Geotechnical and Geoenvironmental Engineering*, 129 (9), 849-857.

Hajiazizi, M., Kilanehei, P. and Kilanehei, F. (2018). "A new method for three dimensional stability analysis of earth slopes", *Scientia Iranica*, 25(1), 129-139.

Hajiazizi, M., Nasiri, M. and Mazaheri, A.R. (2018). "The effect of fixed-tip piles on stabilization of earth slopes", *Scientia Iranica*, 25(5), 2550-2560.

Hajiazizi, M. and Nasiri, M. (2019) "Experimental and numerical investigation of reinforced sand slope using geogird encased stone column", *Civil Engineering Infrastructures Journal*, 52(1), 85-100.

Hajiazizi, M., Mazaheri, A.R. and Orense, R.P. (2018). "An analytical approach to evaluate stability of pile-stabilized slope", *Scientia Iranica*, 25(5), 2525-2536.

Khaled, K.M. and Mahmoud, G.M. (2018). "The influence of the unloading rate on creep recovery of force transducers", *Measurement*, 114, 436-447.

Li, X., Pei, X., Gutierrez, M. and He, S. (2012). "Optimal location of piles in slope stabilization by limit analysis", *Acta Geotechnica*, 7(3), 1369-1383.

Mohamed, M.I., Hasan, E.H. and Aggag, G. (2009). "Study of creep behavior of load cells", *Measurement*, 42(7), 1006-1010.

Oliveira, P.J.V., Santos, S.L., Correia, A.A. and Lemos, L.J. (2019) "Numerical prediction of the creep behaviour of an embankment built on soft soils subjected to preloading", *Computers and Geotechnics*, 114, 103140.

Puzrin, A.M. and Schmid, A. (2012). "Evolution of stabilised creeping landslides", *Geotechnique*, 62 (6), 491-501.

Vulliet, L. and Hutter, K. (1988). "Continuum modes for natural slopes in slow movements", *Geotechnique*, 38 (2), 199-217.

Wang, J., Liu, J., Cao, P., Liang, Q. and Duan, J. (2017) "Coupled creep characteristics of anchor structures and soils under chemical corrosion", *Indian Geotechnical Journal*, 47(4), 521-528.

Wang, P., Liu, E., Song, B., Liu, X., Zhang, G. and Zhang, D. (2019) "Binary medium creep constitutive model for frozen soils based on homogenization theory", *Cold Regions Science and Technology*, 162, 35-42.

Wang, S.h., Wang, J., Wu, W., Cui, D., Su, A. and Xiang, W. (2020) "Creep properties of clastic soil in a reactivated slow-moving landslide in the Three Gorges Reservoir Region, China", *Engineering Geology*, 267, 105493.

Yang, Y., Lai, Y. and Chang, X. (2010). "Experimental and theoretical studies on the creep behavior of warm ice-rich frozen sand", *Cold Regions Science and Technology*, 63, 61-67.

Yao, X., Qi, J., Zhang, J. and Yu, F. (2018) "A one-dimensional creep model for frozen soils taking temperature as an independent variable", *Soils and Foundations*, 58(3), 627-640.

Zhou, X.P. and Cheng, H. (2015). "The long-term stability analysis of 3D creeping slopes using the displacement-based rigorous limit equilibrium method", *Engineering Geology*, 195, 292-300.